frontiers in Molecular Biosciences

ORIGINAL RESEARCH
published: 10 August 2021
doi: 10.3389/fmolb.2021.711975

Simulating PIP_2-Induced Gating Transitions in Kir6.2 Channels

*Michael Bründl, Sarala Pellikan and Anna Stary-Weinzinger**

Department of Pharmaceutical Sciences, Division of Pharmacology and Toxicology, University of Vienna, Vienna, Austria

ATP-sensitive potassium (K_{ATP}) channels consist of an inwardly rectifying K^+ channel (Kir6.2) pore, to which four ATP-sensitive sulfonylurea receptor (SUR) domains are attached, thereby coupling K^+ permeation directly to the metabolic state of the cell. Dysfunction is linked to neonatal diabetes and other diseases. K^+ flux through these channels is controlled by conformational changes in the helix bundle region, which acts as a physical barrier for K^+ permeation. In addition, the G-loop, located in the cytoplasmic domain, and the selectivity filter might contribute to gating, as suggested by different disease-causing mutations. Gating of Kir channels is regulated by different ligands, like $G_{\beta\gamma}$, H^+, Na^+, adenosine nucleotides, and the signaling lipid phosphatidyl-inositol 4,5-bisphosphate (PIP_2), which is an essential activator for all eukaryotic Kir family members. Although molecular determinants of PIP_2 activation of K_{ATP} channels have been investigated in functional studies, structural information of the binding site is still lacking as PIP_2 could not be resolved in Kir6.2 cryo-EM structures. In this study, we used Molecular Dynamics (MD) simulations to examine the dynamics of residues associated with gating in Kir6.2. By combining this structural information with functional data, we investigated the mechanism underlying Kir6.2 channel regulation by PIP_2.

Keywords: molecular dynamics simulations, pore diameter, Kir6.2, PIP2, permanent neonatal diabetes, L164P

OPEN ACCESS

Edited by:
Lei Shi,
National Institutes of Health (NIH), United States

Reviewed by:
Izhar Karbat,
Weizmann Institute of Science, Israel
Ralf Schmid,
University of Leicester, United Kingdom

****Correspondence:***
Anna Stary-Weinzinger
anna.stary@univie.ac.at

Specialty section:
This article was submitted to Structural Biology, a section of the journal Frontiers in Molecular Biosciences

Received: *19 May 2021*
Accepted: *08 July 2021*
Published: *10 August 2021*

Citation:
Bründl M, Pellikan S and Stary-Weinzinger A (2021) Simulating PIP_2-Induced Gating Transitions in Kir6.2 Channels. Front. Mol. Biosci. 8:711975. doi: 10.3389/fmolb.2021.711975

INTRODUCTION

Inwardly rectifying K^+ (Kir) channels are expressed in diverse tissues and regulate physiological processes by setting the cellular resting membrane potential. K^+ efflux is reduced to different degrees due to block by intracellular Mg^{2+} and polyamines at potentials positive to the K^+ equilibrium potential (Ho et al., 1993; Kubo et al., 1993; Nichols and Lee 2018). X-ray and cryo-EM structures of several different Kir family members are available, revealing a remarkably conserved pore architecture, despite widely different ligand gating mechanisms. While all Kir channels require phosphatidylinositol-4,5 bisphosphate (PIP_2) binding for channel activation (Hilgemann and Ball 1996; D'Avanzo et al., 2010; Hansen et al., 2011), gating by many additional ligands is unique. For example, gating of Kir1 and Kir4/5 channels is controlled by pH, Kir3 channels are regulated by $G\beta\gamma$ proteins, and Kir6 by ADP/ATP and sulfonylurea receptor subunits (Nichols and Lopatin 1997).

Recent cryo-EM structures of K_{ATP} channels (Martin et al., 2017a; Martin et al., 2017b; Lee et al., 2017; Li et al., 2017; Wu et al., 2018; Ding et al., 2019) provide important progress towards understanding the complex gating regulation of this important subfamily, which couples the metabolic state of a cell to its electrical excitability (Hibino et al., 2010; Rorsman and Ashcroft 2018). Structures confirm previous expectations that K_{ATP} channels consist of four Kir6.x pore-forming subunits and four regulatory sulfonylurea receptor (SUR) subunits. Like in Kir2 and Kir3 channels, the pore below the selectivity filter (SF) is lined by two main constrictions: the so-called

TABLE 1 | Available Kir6.2 cryo-EM structures in the PDB compared to a pre-open Kir3.2 x-ray structure.

PDB	State	Experimental construct	Ligands in model	Ligands in experiment	Resolution (Å)	r(L164) (Å)	r(F168) (Å)	r(I296) (Å)	Reference
5TWV	Closed	Hamster SUR1, rat Kir6.2	ATP	Glibenclamide, ATP	6.30	1.27	1.66	2.65	Martin et al. (2017b)
6C3P	Closed (*propeller*)	Human SUR1, human Kir6.2 fusion construct	ATP, ADP, Mg^{2+}	ATP, ADP, Mg^{2+}, diC8-PIP_2	5.60	0.97	1.24	2.36	Lee et al. (2017)
6C3O	Closed (*quatrefoil*)	Human SUR1, human Kir6.2 fusion construct	ATP, ADP, K^+, Mg^{2+}	ATP, ADP, Mg^{2+}, diC8-PIP_2	3.90	0.82	1.06	1.59	Lee et al. (2017)
5YW8	Closed	Hamster SUR1, mouse Kir6.2 fusion construct	$ATP_\gamma S$	$ATP_\gamma S$, glibenclamide	4.40	0.84	0.76	2.7	Wu et al. (2018)
5YW9	Closed, (T state, *tense*)	Hamster SUR1, mouse Kir6.2 fusion construct	$ATP_\gamma S$	$ATP_\gamma S$	5.00	0.84	0.76	2.7	Wu et al. (2018)
5YWC	Closed	Hamster SUR1, mouse Kir6.2 fusion construct	ADP, Mg^{2+}	Mg-ADP, VO_4^{3-}, diC8-PIP_2, NN414 (a KCO)	4.30	0.87	0.74	2.64	Wu et al. (2018)
5YWA	Closed, (R state, *relaxed*)	Hamster SUR1, mouse Kir6.2 fusion construct	$ATP_\gamma S$	$ATP_\gamma S$	6.10	0.89	0.71	2.91	Wu et al. (2018)
5YKF	Closed, (T state, *tense*)	Hamster SUR1, mouse Kir6.2 fusion construct	$ATP_\gamma S$, glibenclamide	$ATP_\gamma S$, glibenclamide	4.33	0.82	0.69	2.58	Wu et al. (2018)
5YWB	Closed	Hamster SUR1, mouse Kir6.2 fusion construct	ADP, Mg^{2+}	Mg-ADP, VO_4^{3-}, diC8-PIP_2, NN414 (a KCO)	5.20	0.99	0.62	2.7	Wu et al. (2018)
5YKG	Closed, (R state, *relaxed*)	Hamster SUR1, mouse Kir6.2 fusion construct	$ATP_\gamma S$, glibenclamide	$ATP_\gamma S$, glibenclamide	4.57	0.86	0.59	2.8	Wu et al. (2018)
5YKE	Closed, focus refined TMD + SUR, no CTD	Hamster SUR1, mouse Kir6.2 fusion construct	Glibenclamide	$ATP_\gamma S$, glibenclamide	4.11	0.81	0.5	N/A	Wu et al. (2018)
6BAA	Closed	Hamster SUR1, rat Kir6.2	Glibenclamide, ATP	Glibenclamide, ATP	3.63	1.1	0.46	2.21	(Martinet al., 2017a)
6JB1	Closed, (T state, *tense*)	Hamster SUR1 (Y1209S), mouse Kir6.2 fusion construct	$ATP_\gamma S$, repaglinide, lipids (POPC, PE), digitonin	$ATP_\gamma S$, repaglinide, digitonin, KNtp peptide	3.30	0.96	0.38	2.41	Ding et al. (2019)
5WUA	Closed	Hamster SUR1 (Q608K), mouse Kir6.2	–	Glibenclamide	5.60	1.05	Too narrow	1.5	Li et al. (2017)
3SYA (Kir3.2 ref)	Closed, pre-open	Mouse Kir3.2 crystal structure	diC8-PIP_2, K^+, Na^+	diC8-PIP_2, Na^+	2.98	2.95	2.45	2.96	Whorton and MacKinnon (2011)

The red-white-green color scale of the Resolution column ranges from green (higher resolutions) to red (lower resolutions). Additionally, among the columns for the three pore constriction sites r(L164), r(F168), and r(I296), the colors range from red (narrow pore radii) to green (wider radii).

helix bundle crossing (HBC) gate and the G-loop gate. K^+ flux through K_{ATP} channels is inhibited by direct interactions of the cytoplasmic Kir6 domain with ATP, while Mg-nucleotide binding to SUR also modulates these channels. Furthermore, channel opening is potentiated by PIP_2 binding to Kir6, which reduces channel inhibition by ATP (Baukrowitz et al., 1998; Shyng and Nichols 1998). The molecular determinants of PIP_2 activation in K_{ATP} channels have been investigated in functional studies (Fan and Makielski 1997; Shyng et al., 2000; Cukras et al., 2002; Schulze et al., 2003; Haider et al., 2007; Männikkö et al., 2011; Pipatpolkai et al., 2020). However, structural information of the binding site and the gating transitions leading to channel opening are still missing, since all available cryo-EM structures have been solved in the absence of this activator, even though the molecule was present in some cryo-EM experiments (Lee et al., 2017; Wu et al., 2018) (see **Table 1** for details). This significantly limits our understanding of the molecular mechanisms by which PIP_2 and other ligands regulate these channels.

Functional studies and modeling strongly support a common structural basis for PIP_2 regulation in different Kir family members (Fan and Makielski 1997; Shyng et al., 2000; Cukras et al., 2002; Schulze et al., 2003; Haider et al., 2007; Männikkö

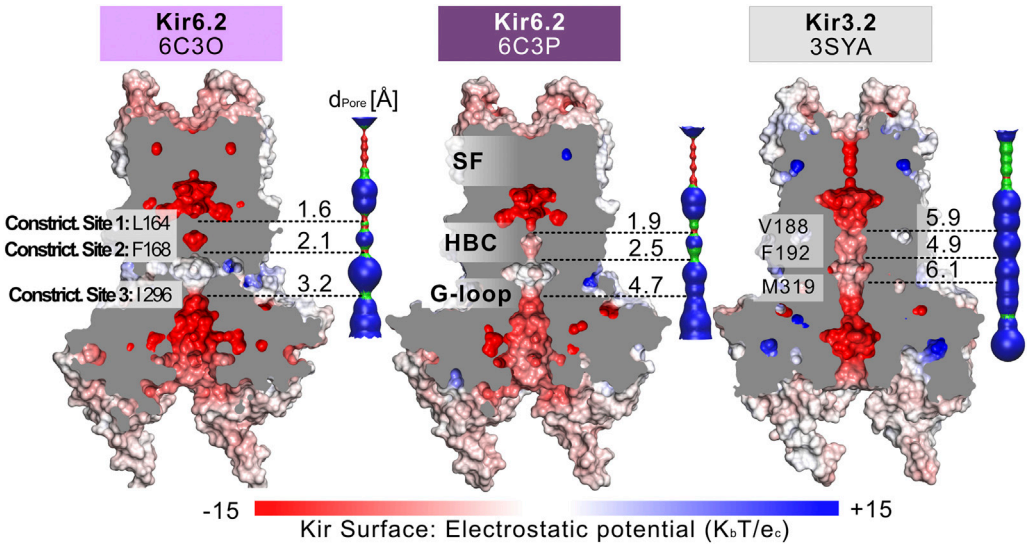

FIGURE 1 | Comparison of the pore dimensions of Kir6.2 structures with Kir3.2. Slices through the pore-forming Kir channel surfaces show three Kir models in the closed state, whereas the pore of Kir3.2 (3SYA) has been described as 'pre-open'. Kir surfaces are colored according to the electrostatic potential. On the right side of each Kir channel, a HOLE profile shows the pore diameter. The three narrowest constriction sites in Kir6.2 below the SF are annotated. In the HOLE profile, red indicates a pore radius too tight for a water molecule. Green suggests space for a single water molecule (0.6 Å < r < 1.15 Å), while blue indicates at least twice the radius of a single water molecule.

et al., 2011; Fürst et al., 2014; Pipatpolkai et al., 2020). Since PIP_2 binding sites are well resolved in Kir2 (Hansen et al., 2011; Lee S. J. et al., 2016; Zangerl-Plessl et al., 2019) and Kir3 channels (Whorton and MacKinnon 2011; Whorton and MacKinnon 2013; Niu et al., 2020), we used this structural information, together with functional data, to investigate the possible structural basis for K_{ATP} channel regulation by PIP_2. Specifically, the aim of the present study was to examine PIP_2-induced gating transitions (after unbinding of ATP from the cytoplasmic domain) using Molecular Dynamics (MD) simulations. Furthermore, we investigated structural changes of the Permanent Neonatal Diabetes mutation (PNDM) L164P that dramatically alters the open state stability of the channel.

RESULTS AND DISCUSSION

Currently Available K_{ATP} Structures Contain Three Constriction Sites

Fourteen cryo-EM structures were resolved to date, with resolutions ranging from 3.3 to 6.3 Å. A complete list of currently available Kir6.2 models with included ligands is given in **Table 1**. To obtain a comprehensive overview of pore dimensions and possible constriction sites, we analyzed pore profiles using the program HOLE (Smart et al., 1996). As shown in **Figure 1** and **Table 1**, three main constriction sites could be identified. Constriction site 1 is located at L164, one helix-turn above the so-called helix bundle crossing (HBC). Constriction site 2, formed by F168 side chains, frames the canonical HBC gate, while I296, a residue associated with the G-loop gate, constitutes the third constriction site. The pore diameter at constriction site one ranges from 0.81 to 1.27 Å, in the respective cryo-EM structures. This is in line with previous studies which identified L164 as a narrow, pore-lining site in Kir6.2 (Loussouarn et al., 2000; Loussouarn et al., 2001; Kurata et al., 2004; Proks et al., 2005; Kurata et al., 2006; Walczewska-Szewc and Nowak 2020). Distances at constriction site 2 range from 0.81 to 1.27 Å, while the pore was slightly wider at I296 (constriction site 3), with distances ranging from 1.5 to 2.9 Å. Overall, none of the structures showed pore radii large enough to enable hydrated K^+ flux through a continuous pore. Even though recent studies suggest that partially dehydrated K^+ ions can pass the HBC gate formed by aromatic side chains (Bernsteiner et al., 2019; Black et al., 2020), the constrictions at sites 1 and 3 are formed by hydrophobic residues, rendering K^+ passage (especially at site 1) very unlikely.

Dynamics of Constriction Sites in MD Simulations

Given our recent success in using MD simulations to provide functional interpretation of conductive states (Bernsteiner et al., 2019; Lee S. J. et al., 2016; Zangerl-Plessl et al., 2019), or mutant-induced gating transitions (Linder et al., 2015), we chose to simulate the pore domain of two Kir6.2 structures. Therefore, we selected PDB accession no. 6C3O and 6C3P (highest-resolution structure pair, solved under identical conditions), acquired in the presence of the Kir6.2 activators Mg-ADP and PIP_2 during the experimental setup (Lee et al., 2017) which have quite different radii at the constriction sites as shown in **Figure 1**. Our recent MD simulations on a Kir3 structure (PDB accession no. 3SYA) revealed that spontaneous wetting of hydrophobic

TABLE 2 | Overview of MD simulations.

Name	n	PIP_2	Length (ns)	Electric field (mV/nm)
6C3O	5	+	1,000	–
6C3O apo	5	–	200	–
6C3P	5	+	1,000	–
6C3P apo	5	–	200	–
6C3P L164P	1	+	1,000	–
6C3P L164P	1	+	1,000	40 (outward)

gates could be obtained in classical, atomistic simulations within relatively short time scales (Bernsteiner et al., 2019). Thus, we performed similar MD simulations with the ATP-unbound, closed pore domains of these Kir6.2 structures after placing short-chain PIP_2 molecules in the respective binding sites, using the 3SYA structure as a template. For details about the setup see **Supplementary Figure S1**. Both, simulating Kir6.2 in the absence of SUR1 (Pipatpolkai et al., 2020), as well as cross-talk analysis between ATP and PIP_2, revealed that removal of SUR1 or ATP (Pipatpolkai et al., 2021) from the cryo-EM structure have a marginal effect on the PIP_2 binding site. Specifically, Pipatpolkai et al. had shown that the presence of ATP primarily influences the dynamics of residue K39 (Pipatpolkai et al., 2021). Comparison of the root-mean-square fluctuations (RMSF) of the PIP_2 binding residues of our simulations (**Supplementary Figure S2**) with those from Pipatpolkai et al. revealed a similar behavior: Simulation setups containing only PIP_2 versus setups with PIP_2 plus ATP suggest no critical bias of our simulations caused by the removal of ATP.

To differentiate the effect induced by PIP_2 from inherent protein dynamics, we compared PIP_2-bound simulations to apo control runs. For simplicity, we will hereinafter refer to these simulations systems as "6C3O" and "6C3P" for the PIP_2-bound WT simulations, and "6C3O apo" and "6C3P apo" for the control runs without PIP_2. See **Table 2** for an overview of simulations.

The stability of the different protein systems, measured as the root-mean-square deviation (RMSD), is shown in **Supplementary Figure S3**. As can be seen in the RMSD plots, all systems reached stable values below 4 Å, which agrees well with previous simulations and a similar system setup (Pipatpolkai et al., 2021).

To assess the pore's lumen at the constriction sites, we monitored the minimum distance of each residue between opposing subunits of 5 × 1 µs simulations over time, as shown in **Figures 2A–C**. L164, forming constriction site 1, sampled minimum distances between fully closed and slightly widened apertures, with average minimum distances of 3.4 and 4.4 Å in 6C3O and 6C3P, respectively. Still, both systems remained not only too narrow for hydrated K^+ ions (6.6 Å (Conway 1981)), but also for water molecules to pass. The pore diameters at the canonical HBC gate were wider in both systems. As shown in **Figure 2B**, a bimodal distribution at F168 caused an asymmetrical pore geometry in both systems. Minimum distances between two opposing subunits frequently sampled 2.6 and 5.8 Å in the 6C3P structure, while the wider pair exhibited distances around 6.7 Å in 6C3O. Despite starting from a narrower HBC gate (2.12 Å diameter), pore diameters increased up to 10 Å in 6C3O, leading to sporadic wetting of the lower HBC gate. However, no persistent wetting in this region could be observed within 1 µs simulation time, as shown in **Supplementary Movies S1, S2**. Summarizing, PIP_2 influences the gate diameter of the HBC gate. This is particularly evident for the 6C3O structure, which occasionally permitted distances wider than the first K^+ solvation shell. The G-loop gate diameter increased in both structures, peaking at 9.3 Å in 6C3O and 10.2 Å in 6C3P, which led to continuous solvation in all simulations (**Figure 2C**, and **Supplementary Movies S1, S2**). Interestingly, no changes could be observed between PIP_2-holo and apo simulations at constriction site 1 (**Supplementary Figure S4**), whereas the bimodal distributions of both systems were shifted towards narrower apertures without bound PIP_2 in constriction sites 2 and 3.

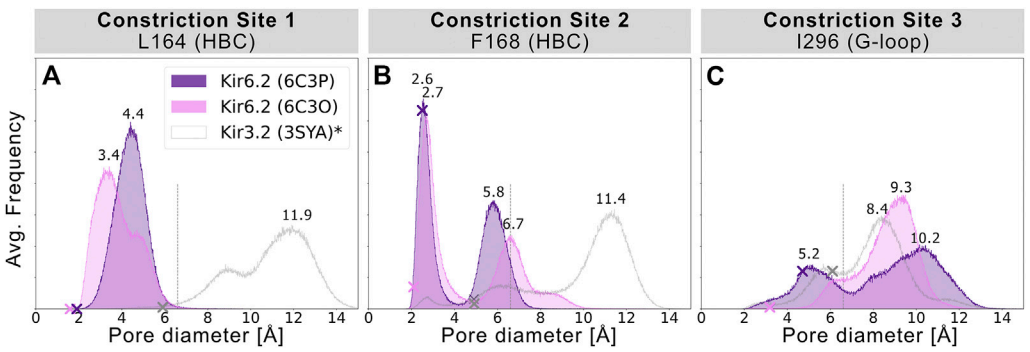

FIGURE 2 | Histograms of pore diameters, sampled in two Kir6.2 systems (6C3O, 6C3P). Minimum distances for three major constriction sites in Kir6.2 were measured in 5 × 1 µs MD simulations for both systems between two opposing subunits and averaged over the number of simulations, subsequently. Crosses mark the corresponding distances of the initial cryo-EM state before equilibration and production run, measured with the HOLE program. A vertical line is drawn at 6.6 Å, indicating the time-averaged hydration diameter of K^+ (Conway 1981). Analogous average minimum-distance values, measured in the G-loop gate (narrowest passage in 3SYA), were associated with conduction in previously published Kir3.2 3SYA simulations (Bernsteiner et al., 2019) (*, gray curve).

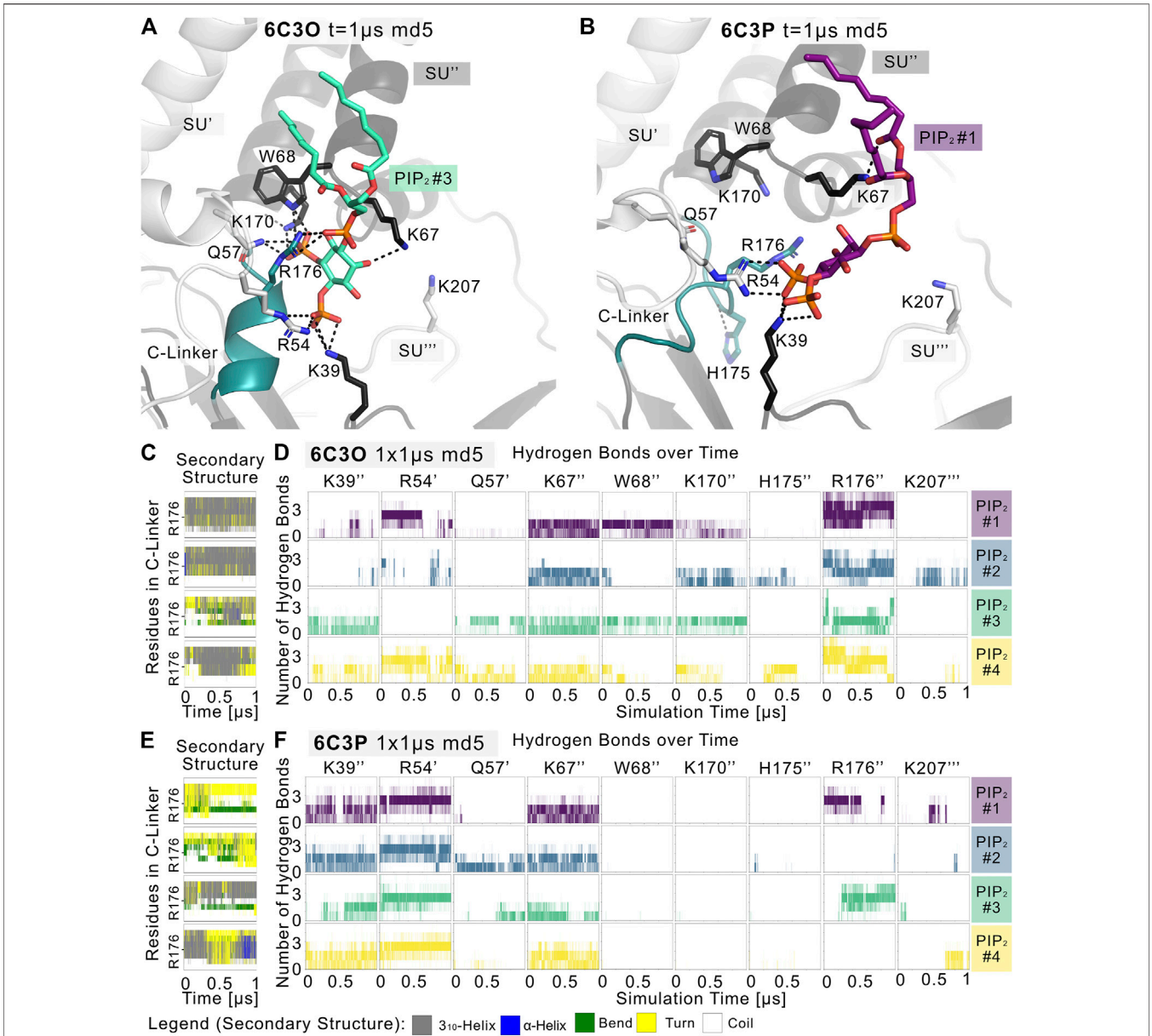

FIGURE 3 | PIP2 binding site and PIP2-induced gating changes. Snapshots of polar Kir6.2-PIP_2 interactions after 1 μs of a representative **(A)** 6C3O and **(B)** 6C3P simulation. Relevant residues are shown as sticks, where colors correspond to a protein subunit (SU). The C-linker is colored in teal. **(C,E)** Plots correspond to four Kir subunits of a representative simulation system. The secondary structure of the **(C)** 6C3O and **(E)** 6C3P C-linkers is shown over time, where the *y*-axis ranges between residues Q173 and T180. The color legend is at the bottom of the figure. **(D,F)** The number of hydrogen bonds is shown between PIP_2 molecules and Kir6.2 residues over time for **(D)** 6C3O and **(F)** 6C3P. Subunits in **(C,D)** and **(E,F)** correspond.

Monitoring PIP_2-Induced Gating Transitions

Given the different behavior of the PIP_2-bound structures in the simulations, we analyzed the structural changes that led to the short-lived wetting and opening transitions at the HBC gate observed in the 6C3O structure. As previously described in structural and functional studies (Hansen et al., 2011; Fürst et al., 2014; Li et al., 2015; Poveda et al., 2017; Niu et al., 2020), we observed a key structural change in the C-linker, characterized by a PIP_2-dependent conversion of the loop into a helix. Thus, we monitored changes in the secondary structure of the C-linker over simulation time in both systems, as shown in **Figures 3C,E**, and subplots A, C, E, G of **Supplementary Figures S5–S7**. Interestingly, there is a ~30% higher helical content (3_{10} helix, corresponding to gray lines in the qualitative plots) in the 6C3O C-linker, compared to 6C3P, suggesting a possible connection between the conformation of the C-linker region and the HBC gate. What might cause this early PIP_2-dependent step towards opening? When comparing residues that render the PIP_2-binding site in 6C3O and 6C3P, a critical difference becomes apparent. R176 was determined to be a key

residue for PIP_2-dependent activation in Kir6.2 (Fan and Makielski 1997; Baukrowitz et al., 1998; Shyng et al., 2000; Haider et al., 2007; Pipatpolkai et al., 2020; Pipatpolkai et al., 2021) and other Kir families (Soom et al., 2001; Lopes et al., 2002; Xie et al., 2005; Lee C. H. et al., 2016; Lacin et al., 2017). As shown in **Figures 3D,F** and **Supplementary Figures S5, S6, S8**, R176 formed stable h-bonds with PIP_2 in all five replicas of the 6C3O system, while h-bonds were missing in one to three subunits of 6C3P simulations. Quantification of PIP_2 occupancies of the two Kir6.2 systems revealed a significant difference for this residue: While R176 was in close distance and formed h-bonds with the PIP_2 head group almost 100% of the time in the 6C3O system, the same interaction was observed only ~50% of the time in the 6C3P system (**Supplementary Figure S8**).

Analysis of the helical content of apo vs. holo runs (**Supplementary Figure S7**) showed a trend for a higher helical content of the C-linker region between holo vs. apo systems in 6C3O. However, only the difference between 6C3O and 6C3P holo systems was statistically significant. Nevertheless, the helical content of the 6C3O holo systems increased slightly with longer sampling times (5 × 1 μs), albeit not statistically significant. This suggests that much longer simulations will be required to sample a more complete picture of the conformational changes in this region.

In agreement with recent simulations (Pipatpolkai et al., 2021), our analyses revealed that PIP_2 binding reduces the dynamics of all binding residues (see **Supplementary Figure S2**). The effect is statistically significant for most residues in 6C3P, whereas the effect on 6C3O was less pronounced. Furthermore, it has previously been shown that K39 plays a critical role for ATP and particularly for PIP_2-dependent interactions. We saw similar effects in our PIP_2 simulations, as shown in **Figures 3D,F** and **Supplementary Figures S2, S5, S6, S8**. However, in contrast to R176, residue K39 seems to play a more general role in stabilizing PIP_2 interactions, independent of HBC gate changes or the helical content of the C-linker, since there is no statistically significant difference of occupancies between the different Kir6.2 systems for this residue. In contrast, significant differences of PIP_2 contacts between 6C3O and 6C3P were observed for residues R54, L66, W68, P69, K170, and R716 (**Supplementary Figure S8**). Combined with the previous observation that a salt bridge between ATP and K39 is broken in the presence of PIP_2, which subsequently leads to a rotation of the K39 amine group towards the PIP_2 head group (Pipatpolkai et al., 2021), this might suggest the following order of gating transition events: In a first step, PIP_2 binding competes with ATP for coordination of the amine group of K39. In a second step, the K39 side chain reorients towards more favorable interactions with PIP_2, thereby reducing ATP inhibition (Hilgemann and Ball 1996; Baukrowitz et al., 1998; Shyng and Nichols 1998; Fan and Makielski 1999). Thirdly, after the release of ATP, h-bonds between R176 and PIP_2 are gradually strengthened, combined with a conformational change of the C-linker and rotational changes of the CTD (see below for discussion), which in turn lead to widening of the gate regions and subsequent ion flux. It will probably require many further simulations, including enhanced sampling techniques in the future to address the exact order of events and kinetics of these processes.

Another important conformational change, reported in several previous studies, concerns the dynamics of the cytoplasmic domain including a rotation of the whole domain (Clarke et al., 2010; Whorton and MacKinnon 2011; Whorton and MacKinnon 2013; Bavro et al., 2012; Li et al., 2015; Li et al., 2017; Linder et al., 2015; Wu et al., 2018; Zangerl-Plessl et al., 2019). We, therefore, monitored the rotation of the CTD over simulation time, as shown in **Supplementary Figure S9**. Indeed, we observed a stronger relative clockwise rotation in the 6C3O simulations (9.2° ± 4.3° std. after 1 μs, n = 5, viewed from the extracellular side), compared to 6C3P. Absolute rotation angles of PIP_2-bound systems converged at ~70° (measured between TMD and CTD of a single protein subunit) in both systems. Nevertheless, fluctuations of the rotation angles render the interpretation of this conformational change rather speculative. Future experiments are necessary to address this question in more detail. Furthermore, an important limitation of our study concerns the lack of the SUR domain, which was not included in our simulation systems, due to the large system size, poor resolution, and many missing residues of these domains. It has to be noted, however, that the N-terminal transmembrane domain of SUR1 modulates PIP_2 sensitivity in Kir6.2 channels (Pratt et al., 2011; Walczewska-Szewc and Nowak 2020). This might explain why no wetting or widening at the uppermost constriction site was observed in our simulations, rendering the channels essentially non-conductive.

Disease Mutation L164P Strongly Influences Pore Geometry

L164P, a mutation targeting constriction site 1, exhibits very high open-state stability and is insensitive to ATP regulation (Enkvetchakul et al., 2000; Loussouarn et al., 2000; Loussouarn et al., 2001). Heterozygous L164P mutations cause permanent neonatal diabetes by significantly increasing intrinsic open probability (Po) compared to WT channels, while retaining single-channel current amplitudes (Flanagan et al., 2006; Tammaro et al., 2008). To investigate proline-induced structural changes on the pore we performed MD simulations of the mutant, using the 6C3P system after 1 μs simulation time (**Figure 4A**). As the mutation targets constriction site 1, which stayed closed and desolvated in our previous WT simulations, we expected pronounced effects on this gating region. Indeed, **Figures 4B,C** and **Supplementary Movie S3** already show changes in pore solvation during a 1 μs simulation. Due to the lack of the hydrophobic side chain, the minimum distance at constriction site 1 increased to ~10 Å, leading to rapid solvation of the cavity above residue F168 (**Figure 4D**). **Figure 4E** shows a shift of the bimodal distribution towards wider average minimum distances (~6.2 Å). Subsequently, constriction site 2 wetted spontaneously with intermittent desolvated periods in both mutant replicas (see **Supplementary Movie S3**). Furthermore, the G-loop gate stabilized in an open and fully solvated conformation, peaking at ~10 Å (**Figure 4F**). To examine

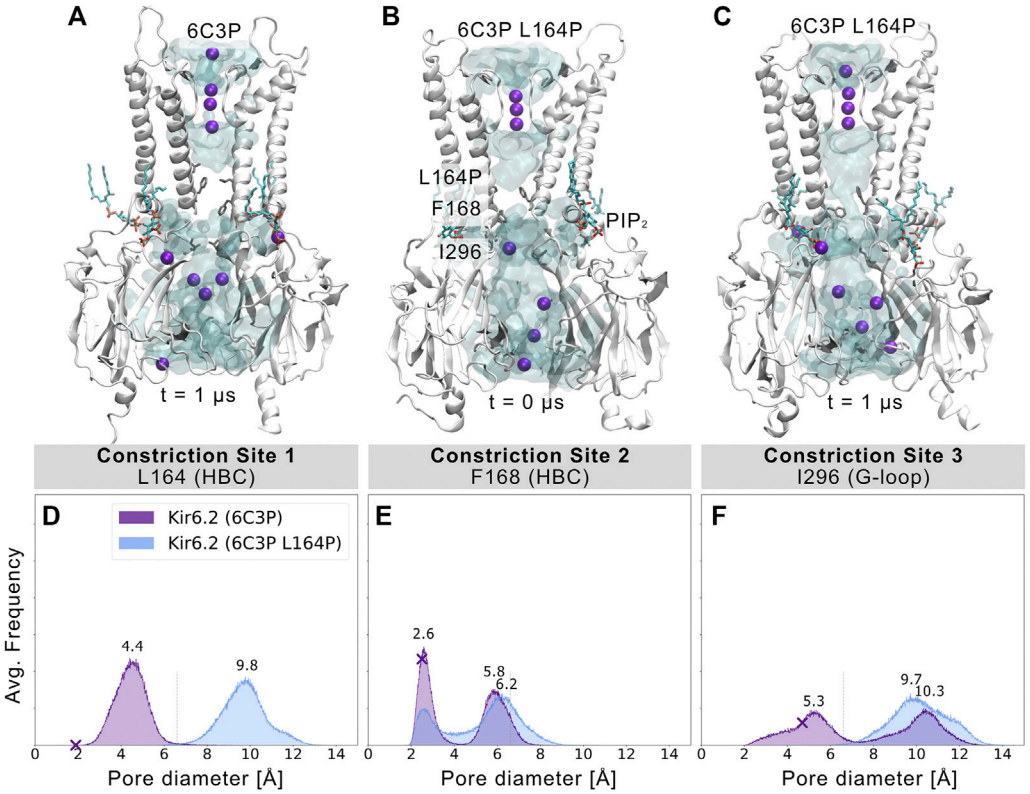

FIGURE 4 | L164P leads to widening of the gates and pore solvation. Snapshots of **(A)** a WT 6C3P system and the equilibrated mutant system 6C3P L164P **(B)** before and **(C)** after 1 µs simulation show the solvation state of the HBC gate. The G-loop gate stabilized fully in an open conformation. **(D–F)** As described in **Figure 2**, histograms of pore diameters show minimum distances for the three major constriction sites of 6C3P and 6C3P L164P. Constriction sites one and three sampled distances wider than the time-averaged hydration diameter of K^+ in the mutant system. The bimodal distribution at constriction site two shifts towards wider apertures, leading to intermittent solvation of the HBC gate. Distances were measured in 2 × 1 µs MD simulation for both systems between two opposing subunits and averaged over the number of simulations, subsequently.

whether the effect on the HBC gate was already enough to facilitate ion conduction, we set up a control replica with a 40 mV nm^{-1} outward driving force. While the simulation revealed a marked effect on the HBC gate, 1 µs sampling time was still not enough to allow continuous K^+ permeation through the whole pore, probably requiring longer sampling times in future studies.

Since proline is known to induce kinks in helices (Cordes et al., 2002), we analyzed the maximum helix angle along the length of the M2 helix over time. **Supplementary Figure S10** shows a significant increase in the maximum M2 helix angle from ~10° to more than 15° on average between 6C3P WT and L164P mutant simulations. This kinking of M2 helices and the lack of the hydrophobic side chain at constriction site 1 led to a widening of the pore. Given the fact that previous studies reported that mutating L164 to cysteine, alanine, valine, threonine or glycine also leads to a large increase in Po (Enkvetchakul et al., 2000; Enkvetchakul et al., 2001; Loussouarn et al., 2000; Loussouarn et al., 2001), this suggests that pore geometry and hydrophobicity at these sites are critical parameters for keeping the pore closed, independent of allosteric ligand effects, such as PIP_2. Unfortunately, mutations at this site can reduce block by drugs such as verapamil (L164C) (Ninomiya et al., 2003) or chloroquine (L164A) (Ponce-Balbuena et al., 2012). Moreover, patients carrying the L164P mutation could not be converted to sulfonylurea therapy. The fact that mutant channels are insensitive to regulation by these drugs, SUR, and ATP (Tammaro et al., 2008) corroborates the relevance of L164 in Kir6.2 gating. Our simulations suggest a link between increased open probability and changed pore geometry. Nevertheless, future studies, including docking and drug screening, will be necessary to address this issue in more detail.

CONCLUSION

Our study provides mechanistic insights into how PIP_2 influences the narrow constriction sites observed in Kir6.2 cryo-EM structures and unravels first structural changes induced by the permanent neonatal diabetes mutation L164P on an atomistic level.

Based on our simulations and recently published simulations on ATP-PIP_2 interactions (Pipatpolkai et al., 2021), we propose the following order of gating events in the Kir6.2 pore region:

In a first step, a salt bridge between ATP and K39 is broken in the presence of PIP_2, which subsequently leads to a rotation of the K39 amine group towards the PIP_2 head group (Pipatpolkai et al., 2021). This is followed by a gradual strengthening of the h-bonds between R176 and PIP_2 upon release of ATP (our current study). In addition, a conformational change of the C-linker and rotational changes of the CTD will lead to widening of the gate regions and will promote subsequent K^+ ion flux (not yet seen in simulations).

Future studies are necessary to obtain a more complete picture, particularly including SUR subunits. This will, however, require higher resolution structures of these regions and much longer sampling times which are beyond the scope of the current paper.

MATERIALS AND METHODS

Pore Analysis With HOLE

Available molecular assemblies of Kir6.2 from the PDB (Research Collaboratory for Structural Bioinformatics Protein Data Bank (RCSB PDB), RRID:SCR_012820) (see **Table 1**), were aligned with the Swiss-PdbViewer (Swiss-PdbViewerDeepViewv4.0, RRID:SCR_013295) (Guex and Peitsch 1997) at the selectivity filter motif TTIGYG. Hydrogens were added to the pore-only files with the help of the APBS-PDB2PQR web server (Adaptive Poisson-Boltzmann Solver, RRID:SCR_008387) (Baker, 2001; Dolinsky et al., 2004) with standard settings (pH 7.0, PARSE FF, internal naming scheme, neutral N and C termini). Slices through the pore-forming Kir channel surfaces were generated with PyMOL (PyMOL, RRID:SCR_000305) (Schrödinger 2015). The surface is colored according to the APBS map with a grid spacing of 0.5. The pqr files were used to calculate the pore dimensions of the Kir channels with the HOLE program (version 2.0) (Smart et al., 1996). Standard settings were used, with pore ending radii (endrad) of 6 Å in channels. The HOLE pore geometry was analyzed with Matplotlib (MatPlotLib, RRID: SCR_008624) (Hunter 2007) and visualized with VMD (Visual Molecular Dynamics, RRID:SCR_001820) (Humphrey et al., 1996).

MD Simulations

Four short-chain C8-PIP_2 molecules were inserted in both Kir6.2 systems (PDB accession no. 6C3O and 6C3P) based on the respective binding conformations, using the 3SYA structure (Whorton and MacKinnon, 2011) as a template. For details about the process see **Supplementary Figure S1**. PIP_2 parameters were taken from our previous work (Lee S. J. et al., 2016). For our MD simulations, we used the amber99sb force field (Hornak et al., 2006) with Berger lipid parameters (Berger et al., 1997). A cut-off of 1.0 nm was employed for Lennard-Jones and electrostatic interactions and long-range interactions calculated with the Particle-Mesh Ewald algorithm (Essmann et al., 1995). The LINCS algorithm (Hess et al., 1997) was used for bond constraints, allowing for an integration time step of 2 fs. V-rescale was used to couple the temperature to 310 K, with a coupling constant of 0.1 ps. The pressure was kept constant semi-isotropically at 1 bar, using the Parrinello-Rahman barostat with τ = 2 ps (Parrinello and Rahman 1981).

Protein topologies were created with the Gromacs module pdb2gmx (Abraham et al., 2018). The PIP_2-bound or apo 6C3O structure was placed in the pre-equilibrated POPC (1-palmitoyl-2-oleoyl-sn-glycero-3- phosphocholine) membrane of our Kir3.2 system (Bernsteiner et al., 2019), containing 588 lipids. K^+ ions were placed at selectivity filter positions (0,2,4), separated by water molecules. After solvation with 82,131 water molecules (SPC/E) (Berendsen et al., 1987) and neutralization with K^+ ions, 150 mM KCl was added to the simulation system. The energy was minimized (steepest descent) in all setups, followed by 1 ns NVT and at least 10 ns NPT equilibration until convergence of temperature and pressure, with restraints on protein atoms to their starting positions (force constant of 1,000 kJ mol^{-1} nm^{-2}). 6C3P systems were set up in the same way, while the L164P mutation was introduced into Kir6.2 with the Swiss PdbViewer (Guex and Peitsch 1997). We chose 6C3P for the mutation, as the model exhibited a wider pore geometry at the cryo-EM state. Gromacs version 2018.8 (GROMACS, RRID:SCR_014565) (Abraham et al., 2015; Abraham et al., 2018) was used to perform all-atomistic MD simulations (see **Table 2** for an overview). In a single 6C3P L164P simulation an electric field of 40 mV nm^{-1}along the *z*-axis of the simulation box was applied to test K^+ conductivity. With a simulation system size of ~17.3 nm in the *z*-direction, this resulted in an electric transmembrane potential of ~700 mV (Treptow and Tarek 2006; Roux 2008). The overall protein stability was assessed by calculating Cα RMSDs with Gromacs after backbone alignment and exclusion of the highly flexible extracellular loop (r97-110) and intracellular C-terminus (r346-359). Figures were rendered with VMD (Humphrey et al., 1996) and PyMol (Humphrey et al., 1996) and movies were produced using Molywood (Wieczór et al., 2020). Maximum helix angles were calculated with the VMD Bendix plugin (Dahl et al., 2012). All data were plotted with Matplotlib (Hunter 2007) and statistical significance was determined using SciPy (Virtanen et al., 2020).

Minimum Distance Analysis

Minimum distances between opposing subunits of pore-forming Kir subunits were calculated with the Gromacs module gmx mindist (Abraham et al., 2018) for residues L164, F168, and I296 in Kir6.2, and corresponding residues in Kir3.2 (V188, F192, M319). The minimum distances of all simulations of a simulation system and both opposing subunits were combined and averaged over the number of simulations.

PIP_2 Binding Site Analysis

We screened the MD trajectories with PyLipid (Song et al., 2021) for residues that were in close proximity (single cutoff: 4 Å) to the PIP_2 headgroup. Residues that formed frequent h-bonds (cut-off angle 30°, cut-off radius: 0.35 nm) between PIP_2 and Kir6.2 were analyzed with the VMD Hydrogen Bonds extension. Selected h-bonds were further analyzed with Gromacs, using the hbond module. The dynamics of residues in the PIP_2 binding site were assessed with the Gromacs module rmsf after aligning the protein along the backbone.

Relative TMD-CTD Rotation

The relative rotation of a single subunit's cytoplasmic domain (CTD) with respect to its transmembrane domain (TMD) was calculated with an in-house script, as described previously (Bernsteiner et al., 2019). The torsional angle was defined by four points: The center of mass (COM) of the TMD's subunit 1 (point 1), the COM of the whole TMD (point 2), the COM of the whole CTD (point 3), and the COM of CTD's subunit 1 (point 4). Kir6.2 residues 53–98 and 116–172 were defined as TMD, while residues 32–52 and 173–346 contributed to the CTD. Thus, the highly flexible extracellular loops in the TMD and the C-termini were excluded for the COM calculations (see **Supplementary Figure S9E**).

Secondary Structure of the C-Linker

The average helical content of the C-linker (= Tether Helix, residues 173–180) was calculated with the Gromacs module do_dssp (Kabsch and Sander 1983; Touw et al., 2015) and was defined as a combination of 3_{10}-helices, α-helices, and π-helices for quantitative analysis.

DATA AVAILABILITY STATEMENT

The original contributions presented in the study are publicly available. This data can be found here: https://doi.org/10.5281/zenodo.4770527.

AUTHOR CONTRIBUTIONS

AS-W designed the study. MB and SP performed simulations. MB, SP, and AS-W analyzed the data. MB and AS-W wrote the paper.

FUNDING

This work was supported by the doctoral program "Molecular drug targets" W1232 of the Austrian Science Fund (FWF; http://www.fwf.ac.at).

ACKNOWLEDGMENTS

The computational results presented have been achieved in part using the Vienna Scientific Cluster (VSC).

SUPPLEMENTARY MATERIAL

The Supplementary Material for this article can be found online at: https://www.frontiersin.org/articles/10.3389/fmolb.2021.711975/full#supplementary-material

REFERENCES

Abraham, M. J., van der Spoel, D., Lindahl, E., and Hess, B.; the GROMACS Development Team (2018). *GROMACS User Manual Version 2018*. https://manual.gromacs.org/documentation/2018/manual-2018.pdf (accessed on 14 July 2021).

Abraham, M. J., Murtola, T., Schulz, R., Páll, S., Smith, J. C., Hess, B., et al. (2015). Gromacs: High Performance Molecular Simulations through Multi-Level Parallelism from Laptops to Supercomputers. *SoftwareX* 1–2, 19–25. doi:10.1016/j.softx.2015.06.001

Baker, N. A., Sept, D., Joseph, S., Holst, M. J., and McCammon, J. A. (2001). Electrostatics of Nanosystems: Application to Microtubules and the Ribosome. *Proc. Natl. Acad. Sci. USA* 98 (18), 10037–10041. doi:10.1073/pnas.181342398

Baukrowitz, T., Schulte, U., Oliver, D., Herlitze, S., Krauter, T., Tucker, S. J., et al. (1998). PIP2 and PIP as Determinants for ATP Inhibition of KATP Channels. *Science* 282 (5391), 1141–1144. doi:10.1126/science.282.5391.1141

Bavro, V. N., De Zorzi, R., Schmidt, M. R., Muniz, J. R. C., Zubcevic, L., Sansom, M. S. P., et al. (2012). Structure of a KirBac Potassium Channel with an Open Bundle Crossing Indicates a Mechanism of Channel Gating. *Nat. Struct. Mol. Biol.* 19 (2), 158–164. doi:10.1038/nsmb.2208

Berendsen, H. J. C., Grigera, J. R., and Straatsma, T. P. (1987). The Missing Term in Effective Pair Potentials. *J. Phys. Chem.* 91 (24), 6269–6271. doi:10.1021/j100308a038

Berger, O., Edholm, O., and Jähnig, F. (1997). Molecular Dynamics Simulations of a Fluid Bilayer of Dipalmitoylphosphatidylcholine at Full Hydration, Constant Pressure, and Constant Temperature. *Biophysical J.* 72 (5), 2002–2013. doi:10.1016/S0006-3495(97)78845-3

Bernsteiner, H., Zangerl-Plessl, E. M., Chen, X., and Stary-Weinzinger, A. (2019). Conduction through a Narrow Inward-Rectifier K+ Channel Pore. *J. Gen. Physiol.* 151 (10), 1231–1246. doi:10.1085/JGP.201912359

Black, K. A., He, S., Jin, R., Miller, D. M., Bolla, J. R., et al. (2020). A Constricted Opening in Kir Channels Does Not Impede Potassium Conduction. *Nat. Commun.* 11 (1), 3024. doi:10.1038/s41467-020-16842-0

Clarke, O. B., Caputo, A. T., Hill, A. P., Vandenberg, J. I., Smith, B. J., and Gulbis, Jacqueline. M. (2010). Domain Reorientation and Rotation of an Intracellular Assembly Regulate Conduction in Kir Potassium Channels. *Cell* 141 (6), 1018–1029. doi:10.1016/j.cell.2010.05.003

Conway, B. E. (1981). *Ionic Hydration in Chemistry and Biophysics*. NetherlandsAmsterdam, Netherlands: Elsevier Scientific Publishing Company.

Cordes, F. S., Bright, J. N., and Sansom, M. S. P. (2002). Proline-Induced Distortions of Transmembrane Helices. *J. Mol. Biol.* 323 (5), 951–960. doi:10.1016/S0022-2836(02)01006-9

Cukras, C. A., Jeliazkova, I., and Nichols, C. G. (2002). The Role of NH2-Terminal Positive Charges in the Activity of Inward Rectifier KATP Channels. *J. Gen. Physiol.* 120 (3), 437–446. doi:10.1085/jgp.20028621

Dahl, A. C. E., Chavent, M., and Sansom, M. S. P. (2012). Bendix: Intuitive Helix Geometry Analysis and Abstraction. *Bioinformatics* 28 (16), 2193–2194. doi:10.1093/bioinformatics/bts357

D'Avanzo, N., Cheng, W. W. L., Doyle, D. A., and Nichols, C. G. (2010). Direct and Specific Activation of Human Inward Rectifier K+ Channels by Membrane Phosphatidylinositol 4,5-Bisphosphate. *J. Biol. Chem.* 285 (48), 37129–37132. doi:10.1074/jbc.C110.186692

Ding, D., Wang, M., Wu, J-X., Kang, Y., and Chen, L. (2019). The Structural Basis for the Binding of Repaglinide to the Pancreatic KATP Channel. *Cel Rep.* 27 (6), 1848–1857. doi:10.1016/j.celrep.2019.04.050

Dolinsky, T. J., Nielsen, J. E., McCammon, J. A., and Baker, N. A. (2004). PDB2PQR: An Automated Pipeline for the Setup of Poisson-Boltzmann Electrostatics Calculations. *Nucleic Acids Res.* 32 (Web Server issue), 665–667. doi:10.1093/nar/gkh381

Enkvetchakul, D., Loussouarn, G., Makhina, E., and Nichols, C. G. (2001). ATP Interaction with the Open State of the KATP Channel. *Biophysical J.* 80 (2), 719–728. doi:10.1016/S0006-3495(01)76051-1

Enkvetchakul, D., Loussouarn, G., Makhina, E., Shyng, S. L., and Nichols, C. G. (2000). The Kinetic and Physical Basis of KATP Channel Gating: Toward a Unified Molecular Understanding. *Biophysical J.* 78 (5), 2334–2348. doi:10.1016/S0006-3495(00)76779-8

Essmann, U., Perera, L., Berkowitz, M. L., Darden, T., Lee, H., and Pedersen, L. G. (1995). A Smooth Particle Mesh Ewald Method. *J. Chem. Phys.* 103 (19), 8577–8593. doi:10.1063/1.470117

Fan, Z., and Makielski, J. C. (1997). Anionic Phospholipids Activate ATP-Sensitive Potassium Channels. *J. Biol. Chem.* 272 (9), 5388–5395. doi:10.1074/jbc.272.9.5388

Fan, Z., and Makielski, J. C. (1999). Phosphoinositides Decrease ATP Sensitivity of the Cardiac ATP-Sensitive K+ Channel: A Molecular Probe for the Mechanism of ATP-Sensitive Inhibition. *J. Gen. Physiol.* 114 (2), 251–269. doi:10.1085/jgp.114.2.251

Flanagan, S. E., Edghill, E. L., Gloyn, A. L., Ellard, S., and Hattersley, A. T. (2006). Mutations in KCNJ11, Which Encodes Kir6.2, Are a Common Cause of Diabetes Diagnosed in the First 6 Months of Life, with the Phenotype Determined by Genotype. *Diabetologia* 49 (6), 1190–1197. doi:10.1007/s00125-006-0246-z

Fürst, O., Mondou, B., and D'Avanzo, N. (2014). Phosphoinositide Regulation of Inward Rectifier Potassium (Kir) Channels. *Front. Physiol.* 4 (404), 1–8. doi:10.3389/fphys.2013.00404

Guex, N., and Peitsch, M. C. (1997). SWISS-MODEL and the Swiss-PdbViewer: An Environment for Comparative Protein Modeling. *Electrophoresis* 18 (15), 2714–2723. doi:10.1002/elps.1150181505

Haider, S., Tarasov, A. I., Craig, T. J., Sansom, M. S. P., and Ashcroft, F. M. (2007). Identification of the PIP2-Binding Site on Kir6.2 by Molecular Modelling and Functional Analysis. *EMBO J.* 26 (16), 3749–3759. doi:10.1038/sj.emboj.7601809

Hansen, S. B., Tao, X., and MacKinnon., R. (2011). Structural Basis of PIP2 Activation of the Classical Inward Rectifier K+ Channel Kir2.2. *Nature* 477 (7365), 495–498. doi:10.1038/nature10370

Hess, B., Bekker, H., Berendsen, H. J. C., and Fraaije, J. G. E. M. (1997). LINCS: A Linear Constraint Solver for Molecular Simulations. *J. Comput. Chem.* 18 (12), 1463–1472. doi:10.1002/(SICI)1096-987X(199709)18:12<1463::AID-JCC4>3.0.CO;2-H

Hibino, H., Inanobe, A., Furutani, K., Murakami, S., Findlay, I., and Kurachi, Y. (2010). Inwardly Rectifying Potassium Channels: Their Structure, Function, and Physiological Roles. *Physiol. Rev.* 90 (1), 291–366. doi:10.1152/physrev.00021.2009

Hilgemann, D. W., and Ball., R. (1996). Regulation of Cardiac Na+, Ca2+ Exchange and KATP Potassium Channels by PIP2. *Science* 273 (5277), 956–959. doi:10.1126/science.273.5277.956

Ho, K., Nichols, C. G., Lederer, W. J., Lytton, J., Vassilev, P. M., Kanazirska, M. V., et al. (1993). Cloning and Expression of an Inwardly Rectifying ATP-Regulated Potassium Channel. *Nature* 362 (6415), 31–38. doi:10.1038/362031a0

Hornak, V., Abel, R., Okur, A., Strockbine, B., Roitberg, A., and Simmerling, C. (2006). Comparison of Multiple Amber Force Fields and Development of Improved Protein Backbone Parameters. *Proteins: Struct. Funct. Bioinformatics* 65 (3), 712–725. doi:10.1002/prot.21123

Humphrey, W., Dalke, A., and Schulten, K. (1996). VMD - Visual Molecular Dynamics. *J. Mol. Graphics* 14 (October 1995), 33–38. doi:10.1016/0263-7855(96)00018-5

Hunter, J. D. (2007). Matplotlib: A 2D Graphics Environment. *Comput. Sci. Eng.* 9 (3), 90–95. doi:10.1109/MCSE.2007.55

Kabsch, W., and Sander, C. (1983). Dictionary of Protein Secondary Structure: Pattern Recognition of Hydrogen-Bonded and Geometrical Features. *Biopolymers* 22, 2577–2637. doi:10.1002/bip.360221211

Kubo, Y., Reuveny, E., Slesinger, P. A., Jan, Y. N., and Jan, L. Y. (1993). Primary Structure and Functional Expression of a Rat G-Protein-Coupled Muscarinic Potassium Channel. *Lett. Nat.* 364 (6440), 802–806. doi:10.1038/364802a0

Kurata, H. T., Marton, L. J., and Nichols, C. G. (2006). The Polyamine Binding Site in Inward Rectifier K+ Channels. *J. Gen. Physiol.* 127 (5), 467–480. doi:10.1085/jgp.200509467

Kurata, H. T., Phillips, L. R., Rose, T., Loussouarn, G., Herlitze, S., Fritzenschaft, H., et al. (2004). Molecular Basis of Inward Rectification: Polyamine Interaction Sites Located by Combined Channel and Ligand Mutagenesis. *J. Gen. Physiol.* 124 (5), 541–554. doi:10.1085/jgp.200409159

Lacin, E., Aryal, P., Glaaser, I. W., Bodhinathan, K., Tsai, E., Marsh, N., et al. (2017). Dynamic Role of the Tether Helix in PIP2-dependent Gating of a G Protein-Gated Potassium Channel. *J. Gen. Physiol.* 149 (8), 799–811. doi:10.1085/jgp.201711801

Lee, C.-H., Huang, P. T., Liou, H. H., Lin, M. Y., Lou, K. L., and Chen, C. Y. (2016). Non-Basic Amino Acids in the ROMK1 Channels via an Appropriate Distance Modulate PIP2 Regulated PHi-Gating. *Biochem. Biophysical Res. Commun.* 473 (1), 303–310. doi:10.1016/j.bbrc.2016.03.100

Lee, K. P. K., Chen, J., and MacKinnon, R. (2017). Molecular Structure of Human KATP in Complex with ATP and ADP. *ELife* 6, e32481. doi:10.7554/elife.32481

Lee, S.-J., Ren, F., Zangerl-Plessl, E. M., Heyman, S., Stary-Weinzinger, A., Yuan, P., et al. (2016). Structural Basis of Control of Inward Rectifier Kir2 Channel Gating by Bulk Anionic Phospholipids. *J. Gen. Physiol.* 148 (3), 227–237. doi:10.1085/jgp.201611616

Li, J., Lü, S., Liu, Y., Pang, C., Chen, Y., Zhang, S., et al. (2015). Identification of the Conformational Transition Pathway in PIP2 Opening Kir Channels. *Scientific Rep.* 5 (11289), 1–12. doi:10.1038/srep11289

Li, N., Wu, J. X., Ding, D., Cheng, J., Gao, N., and Chen, L. (2017). Structure of a Pancreatic ATP-Sensitive Potassium Channel. *Cell* 168 (1–2), 101–110. doi:10.1016/j.cell.2016.12.028

Linder, T., Wang, S., Zangerl-Plessl, E-M., Nichols, C. G., and Stary-Weinzinger, A. (2015). Molecular Dynamics Simulations of KirBac1.1 Mutants Reveal Global Gating Changes of Kir Channels. *J. Chem. Inf. Model.* 55 (4), 814–822. doi:10.1021/acs.jcim.5b00010

Lopes, C. M. B., Zhang, H., Rohacs, T., Jin, T., Yang, J., Logothetis, D. E., et al. (2002). Alterations in Conserved Kir Channel-PIP2 Interactions Underlie Channelopathies. *Neuron* 34 (6), 933–944. doi:10.1016/S0896-6273(02)00725-0

Loussouarn, G., Makhina, E. N., Rose, T., and Nichols, C. G. (2000). Structure and Dynamics of the Pore of Inwardly Rectifying KATP Channels. *J. Biol. Chem.* 275 (2), 1137–1144. doi:10.1074/jbc.275.2.1137

Loussouarn, G., Phillips, L. R., Masia, R., Rose, T., and Colin, G. N. (2001). Flexibility of the Kir6.2 Inward Rectifier K+ Channel Pore. Proceedings of the National Academy of Sciences 98 (7), 4227–4232. doi:10.1073/pnas.061452698

Männikkö, R., Stansfeld, P. J., Ashcroft, A. S., Hattersley, A. T., Sansom, M. S. P., Ellard, S., et al. (2011). A Conserved Tryptophan at the Membrane-Water Interface Acts as a Gatekeeper for Kir6.2/SUR1 Channels and Causes Neonatal Diabetes when Mutated. *J. Physiol.* 589 (13), 3071–3083. doi:10.1113/jphysiol.2011.209700

Martin, G. M., Kandasamy, B., DiMaio, F., Yoshioka, C., and Shyng, S. L. (2017a). Anti-Diabetic Drug Binding Site in a Mammalian KATP Channel Revealed by Cryo-EM. *ELife* 6, 1–27. doi:10.7554/eLife.31054.001

Martin, G. M., Yoshioka, C., Rex, E. A., Fay, J. F., Xie, Q., Whorton, M. R., et al. (2017b). Cryo-EM Structure of the ATP-Sensitive Potassium Channel Illuminates Mechanisms of Assembly and Gating. *ELife* 6, 1–21. doi:10.7554/eLife.24149

Nichols, C. G., and Lopatin, A. N. (1997). Inward Rectifier Potassium Channels. *Annu. Rev. Physiol.* 59 (1), 171–191. doi:10.1146/annurev.physiol.59.1.171

Nichols, C. G., and Lee., S-j. (2018). Polyamines and Potassium Channels: A 25-Year Romance. *J. Biol. Chem.* 293 (48), 18779–18788. doi:10.1074/jbc.TM118.003344

Ninomiya, T., Takano, M., Haruna, T., Kono, Y., and Horie, M. (2003). Verapamil, a Ca 2+ Entry Blocker, Targets the Pore-Forming Subunit of Cardiac Type KATP Channel (Kir6.2). *J. Cardiovasc. Pharmacol.* 42 (2), 161–168. doi:10.1097/00005344-200308000-00002

Niu, Y., Tao, X., Touhara, K. K., and MacKinnon, R. (2020). Cryo-Em Analysis of PIP2 Regulation in Mammalian GIRK Channels. *ELife* 9, 1–18. doi:10.7554/ELIFE.60552

Parrinello, M., and Rahman, A. (1981). Polymorphic Transitions in Single Crystals: A New Molecular Dynamics Method. *J. Appl. Phys.* 52 (12), 7182–7190. doi:10.1063/1.328693

Pipatpolkai, T., Corey, R. A., Proks, P., Ashcroft, F. M., and Stansfeld, P. J. (2020). Evaluating Inositol Phospholipid Interactions with Inward Rectifier Potassium Channels and Characterising Their Role in Disease. *Commun. Chem.* 3 (147), 1–10. doi:10.1038/s42004-020-00391-0

Pipatpolkai, T., Usher, S. G., Vedovato, N., Ashcroft, F. M., and Stansfeld, P. (2021). The Dynamic Interplay of PIP2 and ATP in the Regulation of the KATP Channel. *BioRxiv* [Preprint]. doi:10.1101/2021.05.06.442933

Ponce-Balbuena, D., Rodríguez-Menchaca, A. A., López-Izquierdo, A., Ferrer, T., Kurata, H. T., Nichols, C. G., et al. (2012). Molecular Mechanisms of Chloroquine Inhibition of Heterologously Expressed Kir6.2/SUR2A Channels. *Mol. Pharmacol.* 82 (5), 803–813. doi:10.1124/mol.112.079152

Poveda, J. A., Giudici, A. M., Renart, M. L., Morales, A., and González-Ros, J. M. (2017). Towards Understanding the Molecular Basis of Ion Channel Modulation by Lipids: Mechanistic Models and Current Paradigms.

Biochim. Biophys. Acta - Biomembranes 1859 (9), 1507–1516. doi:10.1016/j.bbamem.2017.04.003

Pratt, E. B., Tewson, P., Bruederle, C. E., Skach, W. R., and Shyng, S-L. (2011). N-terminal Transmembrane Domain of SUR1 Controls Gating of Kir6.2 by Modulating Channel Sensitivity to PIP2. *J. Gen. Physiol.* 137 (3), 299–314. doi:10.1085/jgp.201010557

Proks, P., Girard, C., Haider, S., Gloyn, A. L., Hattersley, A. T., Sansom, M. S., et al. (2005). A Gating Mutation at the Internal Mouth of the Kir6.2 Pore Is Associated with DEND Syndrome. *EMBO Rep.* 6 (5), 470–475. doi:10.1038/sj.embor.7400393

Rorsman, P., and Ashcroft, F. M. (2018). Pancreatic β-Cell Electrical Activity and Insulin Secretion: Of Mice and Men. *Physiol. Rev.* 98 (1), 117–214. doi:10.1152/physrev.00008.2017

Roux, B. (2008). The Membrane Potential and its Representation by a Constant Electric Field in Computer Simulations. *Biophysical J.* 95 (9), 4205–4216. doi:10.1529/biophysj.108.136499

Schrödinger, L. L. C. (2015). "The {PyMOL} Molecular Graphics System, Version~1.8."

Schulze, D., Krauter, T., Fritzenschaft, H., Soom, M., and Baukrowitz, T. (2003). Phosphatidylinositol 4,5-Bisphosphate (PIP2) Modulation of ATP and PH Sensitivity in Kir Channels. A Tale of an Active and a Silent PIP2 Site in the N Terminus. *J. Biol. Chem.* 278 (12), 10500–10505. doi:10.1074/jbc.M208413200

Shyng, S-L., Cukras, C. A., Harwood, J., and Nichols, C. G. (2000). Structural Determinants of PIP2 Regulation of Inward Rectifier KATP Channels. *J. Gen. Physiol.* 116 (5), 599–608. doi:10.1085/jgp.116.5.599

Shyng, S. L., and Nichols, C. G. (1998). Membrane Phospholipid Control of Nucleotide Sensitivity of KATP Channels. *Science* 282 (5391), 1138–1141. doi:10.1126/science.282.5391.1138

Smart, O. S., Neduvelil, J. G., Wang, X., Wallace, B. A., and Sansom, M. S. P. (1996). HOLE: A Program for the Analysis of the Pore Dimensions of Ion Channel Structural Models. *J. Mol. Graphics* 14 (6), 354–360. doi:10.1016/S0263-7855(97)00009-X

Song, W, Corey, R. A., Duncan, A. L., Ansell, T. B., Stansfeld, P. J., and Sansom, M. S. (2021). Pylipid: A Python Toolkit for Analysis of Lipid-Protein Interactions from MD Simulations. *Biophysical J.* Vol. 120, 48a. doi:10.1016/j.bpj.2020.11.532

Soom, M., Schönherr, R., Kubo, Y., Kirsch, C., Klinger, R., and Heinemann, S, H. (2001). Multiple PIP2 Binding Sites in Kir2.1 Inwardly Rectifying Potassium Channels. *FEBS Lett.* 490 (1–2), 49–53. doi:10.1016/S0014-5793(01)02136-6

Tammaro, P., Flanagan, S. E., Zadek, B., Srinivasan, S., Woodhead, H., Hameed, S., et al. (2008). A Kir6.2 Mutation Causing Severe Functional Effects *In Vitro* Produces Neonatal Diabetes without the Expected Neurological Complications. *Diabetologia* 51 (5), 802–810. doi:10.1007/s00125-008-0923-1

Touw, W. G., Baakman, C., Black, J., te Beek, T. A. H., Krieger, E., Joosten, R. P., et al. (2015). A Series of PDB-Related Databanks for Everyday Needs. *Nucleic Acids Res.* 43 (D1), D364–D368. doi:10.1093/nar/gku1028

Treptow, W., and Mounir, T. (2006). Molecular Restraints in the Permeation Pathway of Ion Channels. *Biophysical J.* 91 (3), L26–L28. doi:10.1529/biophysj.106.087437

Virtanen, P., Gommers, R., Oliphant, T. E., Haberland, M., Reddy, T., Cournapeau, D., et al. (2020). SciPy 1.0: Fundamental Algorithms for Scientific Computing in Python. *Nat. Methods* 17 (3), 261–272. doi:10.1038/s41592-019-0686-2

Walczewska-Szewc, K., and Nowak, W. (2020). Structural Determinants of Insulin Release: Disordered N-Terminal Tail of Kir6.2 Affects Potassium Channel Dynamics through Interactions with Sulfonylurea Binding Region in a SUR1 Partner. *J. Phys. Chem. B* 124 (29), 6198–6211. doi:10.1021/acs.jpcb.0c02720

Whorton, M. R., and MacKinnon., R. (2011). Crystal Structure of the Mammalian GIRK2 K+ Channel and Gating Regulation by G Proteins, PIP2, and Sodium. *Cell* 147 (1), 199–208. doi:10.1016/j.cell.2011.07.046

Whorton, M. R., and MacKinnon., R. (2013). X-Ray Structure of the Mammalian GIRK2-Bγ G-Protein Complex. *Nature* 498 (7453), 190–197. doi:10.1038/nature12241

Wieczór, M., Hospital, A., Bayarri, G., Czub, J., and Orozco, M. (2020). Molywood: Streamlining the Design and Rendering of Molecular Movies. *Bioinformatics* 36 (17), 4660–4661. doi:10.1093/bioinformatics/btaa584

Wu, J. X., Ding, D., Wang, M., Kang, Y., Zeng, X., and Chen, L. (2018). Ligand Binding and Conformational Changes of SUR1 Subunit in Pancreatic ATP-Sensitive Potassium Channels. *Protein and Cell* 9 (6), 553–567. doi:10.1007/s13238-018-0530-y

Xie, L. H., John, S. A., Ribalet, B., and Weiss, J. N. (2005). Long Polyamines Act as Cofactors in PIP2 Activation of Inward Rectifier Potassium (Kir2.1) Channels. *J. Gen. Physiol.* 126 (6), 541–549. doi:10.1085/jgp.200509380

Zangerl-Plessl, E-M., Lee, S-J., Maksaev, G., Bernsteiner, H., Ren, F., Yuan, P., et al. (2019). Atomistic Basis of Opening and Conduction in Mammalian Inward Rectifier Potassium (Kir2.2) Channels. *J. Gen. Physiol.* 152 (1), 1–16. doi:10.1085/JGP.201912422

Conflict of Interest: The authors declare that the research was conducted in the absence of any commercial or financial relationships that could be construed as a potential conflict of interest.

Publisher's Note: All claims expressed in this article are solely those of the authors and do not necessarily represent those of their affiliated organizations, or those of the publisher, the editors and the reviewers. Any product that may be evaluated in this article, or claim that may be made by its manufacturer, is not guaranteed or endorsed by the publisher.